

Mechanical properties of additively manufactured metal lattice structures: Data review and design interface



Bradley Hanks*, Joseph Berthel, Mary Frecker, Timothy W. Simpson

Pennsylvania State University, 314 Leonhard Building, University Park, PA 16802, United States

ARTICLE INFO

Keywords:

Powder bed fusion
Lattice structures
Design for additive manufacturing

ABSTRACT

With the ever-increasing resolution of metal additive manufacturing processes, the ability to design and fabricate cellular or lattice structures is readily improving. While there are few limits to the variety of unit cell topologies that can feasibly be manufactured, there is little known about the effect that the underlying unit cell topology has on lattice structure mechanical performance. Increased knowledge of lattice structure performance based on the unit cell topology can aid in appropriate unit cell selection to achieve desired lattice structure mechanical properties. The objective in this work is to compile metal additively manufactured lattice structure characterization data found in the literature into Ashby-style plots that can be used to differentiate unit cell topologies and guide unit cell selection. Data gathered from literature encompasses over 69 papers describing 18 different unit cell topologies. Data on mechanical properties such as the effective modulus, Poisson's ratio, yield strength, buckling strength, and plateau strength, of lattice structures from analytical models based on mathematical derivations, finite element analysis, and experimental characterization was gathered and synthesized. In total, nearly 1650 data points for experimental and finite element analysis were compiled along with a variety of analytical models for 18 different unit cell topologies. The process of gathering the data from the literature along with the assumptions used to compile the data are discussed. A graphical user interface and database were developed that allows for comparison of different lattice structure mechanical properties based on their unit cell topology. The Lattice Unit-cell Characterization Interface for Engineers (LUCIE) provides a simple format to guide engineers, scientists, and others towards understanding the relationships of the unit cell topology and the lattice structure mechanical properties, with the intent of guiding appropriate unit cell selection. Three case studies are shown for using LUCIE to differentiate unit cell topologies for improved understanding of experimental and simulation-based results (Case Study 1), to identify unit cell topology options for reducing weight while maintaining yield stress or increasing yield stress without reducing weight (Case Study 2), and for quickly narrowing multiple options to an appropriate unit cell topology (Case Study 3).

1. Introduction

With the recent growth in additive manufacturing (AM), the interest in printing components for end-use parts is increasing. AM refers to fabrication processes where material is added in a layer-by-layer approach. As AM machines continue to improve the resolution and quality of printed parts, there is growing interest in understanding the resulting mechanical properties to ensure that AM components will perform as needed. In addition, with improved print resolution, more complex structures at the mesoscale are being incorporated into components, requiring additional knowledge and insight regarding the effect that the mesoscale complexity plays on the performance of the component as a whole. The purpose of this paper is to provide a comprehensive

compilation of mechanical properties of non-stochastic AM lattice structures with regular unit cell topologies through an interactive interface.

In AM, mesoscale refers to the intercomponent complexity, specifically feature sizes on the scale of 0.1–10 mm [1]. For comparison, the macroscale defines the overall or bulk geometry of a component. Meanwhile, the microscale encompasses the physical material characteristics such as microstructure, grain size and orientation, material phase, etc. The mesoscale lies in between these two scales, where complexity can be added to the component through lattice structures or other approaches (e.g., the honeycomb structure in the crumple zone of a car or beehive, or the space-filling metal foams used in medical implants).

* Corresponding author.

E-mail addresses: bbh5108@psu.edu (B. Hanks), jtb5656@psu.edu (J. Berthel), mxr36@psu.edu (M. Frecker), tws8@psu.edu (T.W. Simpson).

Nomenclature	
A	Analytical data type
AM	Additive manufacturing
BS	Lattice structure buckling stress normalized by the solid yield stress
E	Experimental data type
EC	Lattice structure compressive elastic modulus normalized by the solid material modulus
F	Finite Element Analysis data type
FEA	Finite Element Analysis
LUCIE	Lattice Unit-cell Characterization Interface for Engineers
PR	Lattice structure Poisson's ratio
PS	Lattice structure plateau stress normalized by the solid yield stress
YS	Lattice structure yield stress normalized by the solid yield stress

A lattice structure is a relatively modern term used in AM to describe the cellular patterns that can be designed and subsequently fabricated into AM components. Examples of lattice structures used today are metallic and non-metallic foams, honeycomb structures, and sandwich panels. Ashby and Gibson [2–5] are well known for their extensive work in the area of cellular materials and the development of mathematical formulations to describe the performance of porous structures. In these types of applications, components or materials can be manufactured with improved stiffness to weight ratios as compared to a solid block of material—and less build time in the case of AM—while maintaining the structural integrity or mechanical properties necessary for the application. While cellular structures have been used for many years, the geometries that can be fabricated have traditionally been limited by conventional manufacturing processes; however, AM is creating renewed interest in the design and use of lattice structures. For instance, a variety of research topics are being explored regarding modeling approaches [6,7], design and optimization [8–11], and experimental testing [12–16] as well as several reviews [17–21] for AM-fabricated lattice structures.

Stochastic lattice structures are a randomized structure such as a metal foam, on the other hand, non-stochastic lattice structures are patterned after a repeated unit cell. The focus in this paper is on non-stochastic lattice structures because the purpose is to identify relationships between the unit cell topology and the effective mechanical properties of the lattice structure. Several different lattice structure classification systems have been proposed with varying levels of detail to cover the infinite possibilities of patternable structures [18,22–24]. The classification system defined by Tamburrino et al. [18] is used for its simplicity in defining 3D unit cell topologies as (1) triply periodic minimal surfaces (TPMS), (2) strut and node arrangement (truss), or (3) custom unit cells. As the focus was on common unit cell topologies for which multiple sources were available, the third category was excluded from this work. Examples of TPMS unit cell topologies include the Schoen gyroid [25,26] and Schwarz diamond [26]. Common examples of truss unit cell topologies are the cube, octet truss, body-centered cubic (BCC), and face-centered cubic (FCC) to name a few (see examples in Fig. 1).

Lattice structures are frequently designed into a component through standard computer-aided design (CAD) modeling software (e.g., SolidWorks, Autodesk Inventor, PTC Creo) or AM-specific software (e.g., Autodesk Netfabb, ANSYS SpaceClaim, nTopology nTop Platform, 3D Systems 3DXpert, Materialise 3-matic). Within the AM-specific software, a library of unit cell topologies to generate different lattice structures or infill patterns are offered; however, their implications on the bulk (i.e. macroscale) mechanical properties of the component are unknown in many cases (e.g., the unit cell topology has inherent mechanical properties in compression and shear that will affect the overall component performance).

Various methodologies have been recommended regarding the design or inclusion of lattice structures in a component [18,27]. Tamburrino et al. [18] discuss unit cell selection based on the choice of either a stretched-dominated or a bending-dominated lattice structure [18]. However, grouping all truss-based lattice structures into these two categories without distinguishing further essentially leaves the decision

wide open. In recent work by Bhate [27], the first of four questions regarding cellular material design is, “What is (are) the optimum unit cell(s)?” [27]. Bhate describes several methods that have been explored in the literature, namely, Maxwell's stability criterion, Gibson-Ashby models of cellular materials, computational analysis, and experimental testing.

In a recent publication, Maconachie et al. [28] provide an extensive review of topics surrounding SLM lattice structures. The topics include types of lattice structures and their applications, processing parameters, microstructure and mechanical properties, numerical modeling, experimental approaches, and outstanding challenges. As discussed in the review, with all the current research into lattice structures, there is a need to compile and provide a comprehensive analysis of the data available. This review does compile some experimental data, nonetheless, a comprehensive compilation of metal AM lattice structure performance data in literature does not exist.

In order to expand the current understanding of lattice structure properties and to improve unit cell selection, this work seeks to compile reported mechanical properties for non-stochastic AM lattice structures of regular unit cell topologies, gathered through analytical modeling, finite element analysis (FEA), and experimental testing. The gathered data is compiled and illustrated in Ashby-style plots through the Lattice Unit-cell Characterization Interface for Engineering (LUCIE), a graphical user interface that allows researchers to easily compare mechanical properties of metal lattice structures based on different unit cell topologies made with AM. Similar to traditional material selection through Ashby plots, this work seeks to make lattice structure selection available through scatter plots with axes chosen based on lattice structure properties. The primary intent is not to provide exact mechanical property values, but instead provide visualization of performance trends based on the unit cell topology.

Section 2 describes the method for gathering, evaluating, and preparing the lattice structure data. Section 3 shows three case studies with LUCIE to compare reported data in literature as well as a case study of how LUCIE can be used to guide unit cell selection. Next, in Section 4, analysis of the outcomes and current limitations of the data and graphical interface are discussed. Finally, Section 5 concludes with a summary of the progress and future work to be performed.

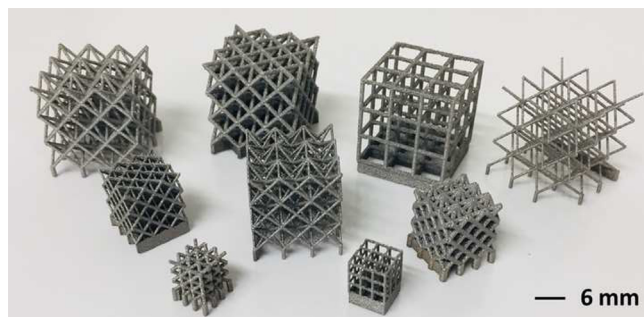


Fig. 1. AM lattice structures produced using laser powder bed fusion in Ti64.

2. Methods

In this section, the methods for identifying relevant research articles, gathering and storing data, visualizing the data, as well as assumptions made during data collection are described. A graphic summary of the methods section is shown in Fig. 2.

2.1. Literature compilation

In order to identify research articles containing relevant lattice structure data, literature searches were conducted in multiple databases such as Compendex. The primary goal of the search was to find research articles from theses, dissertations, conference, and refereed journal articles containing mechanical performance information of metal lattice structures made with AM powder bed fusion (laser or electron beam).

With the recent increase in research in AM, there is still a wide variety of terms to describe similar if not the same concepts. In recent years, the term "lattice structure" has become more common, though additional terms such as "metamaterial", "cellular structure", or "mesoscale design" are also used, often interchangeably. In addition to these search terms regarding the lattice structure, there are a variety of search terms for the manufacturing process including "additive manufacturing", "rapid prototyping", "3D printing", etc. More specific to this paper, the search was for metal AM such as, "powder bed fusion", "selective laser melting", "direct metal laser sintering", and "electron beam melting". In order to narrow the wealth of papers that these search terms can produce, other search terms such as "mechanical performance", "mechanical characterization", "mechanical properties", etc. were included. No restrictions were placed on publication year of the source. While the intent was to gather all published literature articles containing mechanical characterization of metal lattice structures made with AM, it became difficult to find all current and relevant

literature due to a wide variety of terminology included in today's research articles. In various combinations, the aforementioned keywords were searched using Google Scholar and Compendex. Additional references were also found through snowballing, a technique for expanding literature reviews through exploration of relevant sources cited within the compiled literature findings.

From each paper, three main data types were considered for inclusion: (1) analytical models, (2) FEA, and (3) experimental. These three data types are defined as follows.

Analytical data is defined here as mechanical performance or properties derived from mathematical equations based on structural shear/normal forces or bending moments. For example, papers that were grouped into the analytical category were often derived using beam theory, considering each individual strut within the unit cell topology. The result of the papers in the analytical category was a continuous equation, generally relying on unit cell size and volume fraction as inputs or independent variables and the predicted mechanical property being the dependent variable.

Papers grouped in the FEA category are defined in terms of mechanical performance or properties gathered through modeling and simulation of individual or arrayed unit cells. This data was available in research articles as either data points or extracted using a power law regression fit. Key features of this data type were the requirement to have full information regarding unit cell topology, volume fraction or strut diameter, and material. In order to normalize all results, raw data was divided by the corresponding bulk, or solid, mechanical property. In cases where the reported data was not normalized, or where the bulk mechanical property was not given in the source, the raw data was normalized using the mechanical property values shown in Table 1.

Finally, papers in the experimental category are defined in terms of mechanical performance or properties determined based on experimental testing of metal AM-fabricated lattice structures. Experimental data was available in published literature as data points in tables and on graphs. In some sources these data points represented an average from multiple tests; however, in other sources, data points for all replicates in the experiment were reported as opposed to a single average value. Similar to the FEA category, a clear description of the geometry, volume fraction, and, where possible, as-built mechanical properties of solid material specimens were gathered. In some cases, as-built strut diameter or volume fraction were reported; however, nominal, or as-designed, values were also collected for consistency. As with the FEA data type, if the reported data was not normalized, then the mechanical properties from Table 1 were used to normalize the data.

After gathering 117 research articles from the literature search, the total number of articles was reduced to 69 using the following criteria:

- Paper must contain mechanical properties for quasi-static compressive behavior
- Paper must contain a clear depiction of unit cell topology through figures, pictures, and/or textual description
- Paper must contain a clear description of unit cell volume fraction (or porosity)
- Paper must contain data for a standard/common unit cell topology (available in at least one additional source)

A more detailed breakdown of how the research articles were reduced is as follows. The total number of articles was reduced from 117 to 109 by first removing those which were duplicates, or reported data repeated in other sources. Next the total number of articles was reduced to 92 by considering only those containing lattice structure mechanical performance and properties for quasi-static compressive behavior. Though a few instances of lattice structure test data for tensile, shear, bending, or combined loading conditions were found in the literature, the data is extremely limited, and as such, only quasi-static compressive characterization data is included in this work [31–35]. For other types of loading conditions, information regarding lattice structure fatigue

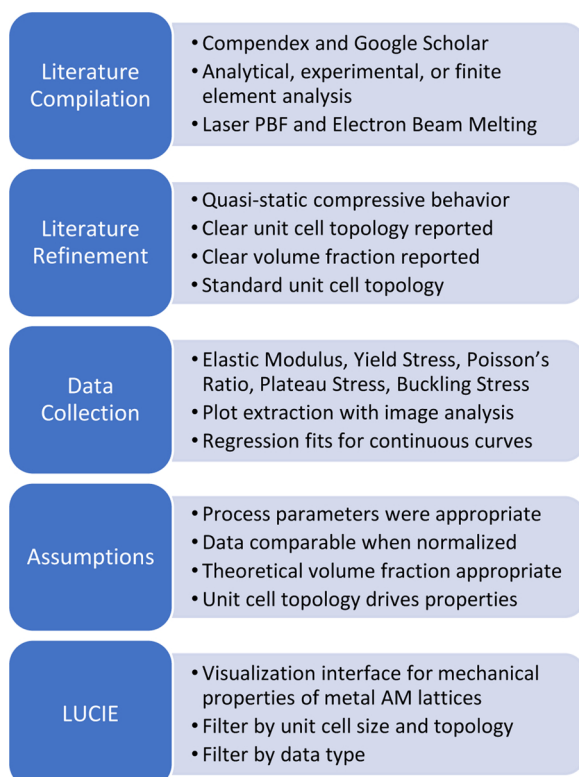


Fig. 2. Graphic summary of the methods section including how sources were found and refined, data collection and assumptions made, and finally incorporation into LUCIE.

Table 1

For sources without bulk mechanical properties of the as-built material, reported within the source, these generic AM mechanical property values were used to normalize data to create a material independent comparison of unit cell topology.

AM Material	Elastic Modulus (GPa)	Yield Stress (MPa)
Co-Cr [29]	200	1060
AlSi10Mg [29]	75	270
Ti64 [30]	129	1007
SS 316 L [29]	185	530
Hastelloy X [29]	195	630

performance or high-strain deformation is recently becoming available (c.f. [36–41],) but is not included in this work. The selection of papers was further reduced to 69 due to insufficient information such as an ambiguous depiction of the unit cell topology or volume fraction and non-standard unit cell topologies for which little data was available [15,42,43]. Similarly, in some cases, part of the data was excluded based on the limited data available on a unique topic, such as how the aspect ratio or rotation of the unit cell topology affects mechanical properties [13,44–46]. In general, data was collected that considered regularly shaped unit cells, often cubic, that could be scaled by adjusting the unit cell size or densified by increasing the thickness of struts or walls.

After the literature search and filtering, metal AM lattice structure data was obtained from a total of 69 papers. Table 2 shows the references and a summary of the unit cell topology, material, and the data type gathered from the paper. In the table, the properties are abbreviated as compressive elastic modulus (EC), yield stress (YS), Poisson's ratio (PR), plateau stress (PS), and buckling stress (BS). Each of these properties are defined in the context of this work in the results section (see Section 3). The data types are abbreviated as analytical (A), FEA (F), and experimental (E).

2.2. Data collection

Data was collected from the 69 papers that provided all of the required mechanical property information for lattice structure characterization. The volume fraction of the tested unit cell topology was required to compare data from different sources. Additionally, for experimental and FEA data, the material needed to be given in order to normalize all the data. As noted earlier, data was normalized by dividing the reported property value of the lattice structure by the bulk mechanical property for the as-built material. Normalization allowed comparison of data taken from sources using different materials.

Data collection depended on how each paper presented their findings. If data was explicitly reported as numerical values, then those values were simply catalogued along with the other required information. In some cases, numerical data was not provided, and plotted graphs were given instead. To extract the relevant data points, WebPlotDigitizer [107] was used to find the approximate values of the plotted data. WebPlotDigitizer is a web-based image analysis tool specifically designed to extract data from images of graphs and plots. The accuracy of the extracted data is dependent on the figure image quality within the cited source and on the user error in precisely selecting data points from the extracted image. WebPlotDigitizer has been recognized as a viable method for data collection when the raw data is unavailable. Several studies have been performed to verify and validate the use of such digital image data collection tools [108–110]. Though digital image extraction of data points introduces uncertainty, one study [109] reported that WebPlotDigitizer resulted in a Lin's concordance value of 0.982, for which 0.99–1 is considered a near-perfect match [111]. From these studies, the extracted data was found to be reliable, valid, have little absolute difference from the true values, and have excellent consistency.

Meanwhile, in eight FEA data type sources [34,56,61–65,88], instead of reporting specific simulation data points, the data was reported as points connected by line segments, i.e., a segmented curve. Though in some cases a slight and sudden change in slope indicated the likelihood of a data point, it was not possible to identify each of these data points on all plots. Because individual points of the FEA simulation could not be distinguished, a power law regression fit was used to match the segmented curve as best as possible and extract the data from the graph. The regression fit of these segmented curves will introduce some additional error; however, *the primary intent of LUCIE is not to provide an exact mechanical property value, but to provide property trends based on the unit cell type*.

The power law regression is based on a popular property-volume fraction model for cellular structures by Gibson and Ashby [4], where P is the property, V_f is the volume fraction, and a, b are constants determined by the fit of the model to the experimental data; see Eq. 1.

$$P = a(V_f)^b \quad (1)$$

A modified power regression equation, with an additional constant, c , was used specifically for the Poisson's ratio property, ν , to better match data that did not intersect the origin (see Eq. 2). For these eight sources with segmented curves, instead of individual data points, WebPlotDigitizer was first used to extract data points along the curve. Second, the power law regression fit coefficients for the extracted points were solved using Desmos [112]. Desmos is an online graphing calculator that can fit a regression model to a set of data points.

$$\nu = a(V_f)^b + c \quad (2)$$

2.3. Assumptions for comparing data

In order to compare data from different papers, many assumptions had to be made. Data was collected only from papers that tested metal prints made with laser or electron beam powder bed fusion processes. It was assumed that all types of metallic materials and the printing process parameters were valid. We also assumed that data from different metallic powder feedstock was comparable when normalized (e.g., different suppliers provide equivalent grades of Ti-6Al-4 V feedstock). Where possible, the normalized value was calculated using the mechanical property of the as-built material reported in the paper. In cases where the as-built material was not experimentally characterized or given in the paper, bulk values were chosen from published data sheets. The mechanical property values of different materials built with AM are given in Table 1.

Additionally, we assumed that all methods of testing, both experimental and FEA, and analytical derivations can be compared. For FEA and analytical data, it was assumed that unit cell size does not influence mechanical properties. This may seem like a limiting assumption, but in many cases, papers did not report unit cell size for analytical models or FEA simulations. For experimental data, unit cell size was recorded if it was given in the source. For analytical data specifically, it was assumed that the derivations for volume fraction consider strut overlap and are accurate. For many papers, data was extracted from plots, and it was assumed that data taken from plots are valid within the resolution available. Though some papers measured the actual volume fraction, or relative density, of the AM lattice structures, the theoretical volume fraction, or as-designed value, was used in this work because it was reported more consistently in literature.

The potential sources of error include: experimental error within the reported results, low image quality in figures used to extract data points with WebPlotDigitizer, human error in precisely selecting data points in an image when gathering data, and the regression fits of the segmented curves for some of the FEA data type data. While there are several potential sources of error, the total error is assumed to be minimal when combining data from so many different models and experiments

Table 2

Summarized list of all sources for data compiled in LUCIE. In this table the unit cell topology, properties recorded, and data type available are sorted by source.

Author	Unit Cell Topology	Property	Data Type	Material
Ahmadi [47]	Diamond	EC, YS, PR, BS, PS	A, E, F	Ti-6Al-4V
Ahmadi [12]	Cubic, Diamond, Truncated Cube, Truncated Cuboctahedron, Rhombic Dodecahedron, Rhombicuboctahedron	EC, YS, PS	E	Ti-6Al-4V
Arabnejad [48]	Octet-Truss	EC, YS	E	Ti-6Al-4V
Ataei [49]	TPMS Gyroid	EC, YS, PS	E	CP-Ti
Beyer [50]	BCC	YS	E	AlSi10Mg
Bobbert [51]	TPMS Gyroid, TPMS Diamond	EC, YS	E	Ti-6Al-4V
Borleffs [52]	Cubic, Diamond, Rhombic Dodecahedron, Truncated Octahedron	EC, PR	A, F	Ti-6Al-4V
Campanelli [53]	FCCZ	YS, PS	E	Ti-6Al-4V
Cheng [54]	Rhombic Dodecahedron	EC, YS	E	Ti-6Al-4V
Choy [13]	Cubic	EC, PS	E	Ti-6Al-4V
de Formanoir [55]	Octet-Truss	EC	E	Ti-6Al-4V
Deshpande [46]	Octet-Truss	EC, YS	A	n/a
Gümruk [56]	BCC	EC, YS	E, F	SS 316 L
Gümruk [33]	BCC, FCCZ, F2BCC	EC, YS	E	SS 316 L
Han [57]	Cubic, BCC	EC, YS	E, F	Co-Cr
Harrysson [58]	Rhombic Dodecahedron	EC, YS	E, F	Ti-6Al-4V
Hasib [59]	Octahedron, Rhombic Dodecahedron	EC, YS	E	Ti-6Al-4V
He [60]	Octet-Truss	EC, YS	A	n/a
Hedayati [34]	Cubic, Truncated Octahedron, Rhombic Dodecahedron, Diamond	EC, YS, PR	F	Ti-6Al-4V
Hedayati [61]	Rhombicuboctahedron	EC, YS, PR	A, E, F	Ti-6Al-4V
Hedayati [62]	Truncated Cube	EC, YS, PR, BS	A, E, F	Ti-6Al-4V
Hedayati [63]	Cubic, Rhombic Dodecahedron, Diamond, Truncated Octahedron	EC, YS, PR	A, F	Ti-6Al-4V
Hedayati [64]	Truncated Cuboctahedron	EC, YS, PR	A, F	Ti-6Al-4V
Hedayati [65]	Octahedron	EC, PR	A, F	Ti-6Al-4V
Heinl [66]	Diamond	EC, YS	E	Ti-6Al-4V
Heinl [67]	Diamond	EC, YS	E	Ti-6Al-4V
Helou [68]	TPMS Gyroid, TPMS Diamond	EC	E, F	SS GP1
Hussein [69]	TPMS Gyroid, TPMS Diamond	EC, YS	E	Ti-6Al-4 V, AlSi10Mg, SS 316 L
Leary [70]	BCC, FCCZ, FCC, FCCZ, F2BCC	EC, YS	E	AlSi12Mg
Leary [14]	BCC, FCCZ, FCC, FCCZ	EC, YS	E	Inconel 625
Lei [71]	BCC, FCCZ	EC, YS	E, F	AlSi10Mg
Li [72]	BCCZ	EC	A	AlSi10Mg
Li [73]	Cubic, Rhombic Dodecahedron, G7	EC, PS	E	Ti-6Al-4V
Liu [74]	Rhombic Dodecahedron	EC	E	Ti2448
Liu [75]	Rhombic Dodecahedron	EC	E	Ti2448
Mazur [76]	BCC, FCC, F2BCCZ	EC, YS	E	Ti-6Al-4V
McKown [39]	BCC, FCCZ	EC, YS, PR	E	SS 316 L
Mines [77]	BCC	EC, YS	E	Ti-6Al-4V
Mullen [78]	BCC	YS	E	CP-Ti
Murr [79]	Rhombic Dodecahedron	EC	E	Co-Cr
Murr [80]	Cubic, Rhombic Dodecahedron, G7	EC	E	Ti-6Al-4V
Murr [81]	Rhombic Dodecahedron	EC	E	Inconel 625
Ozdemir [40]	Diamond	EC, YS	E	Ti-6Al-4V
Parthasarathy [82]	Cubic	EC, YS	E	Ti-6Al-4V
Ptochos [83]	BCC	EC, PR	A	n/a
Rehme [84]	FCC, FCCZ, BCC, FCCZ, F2BCC, F2BCCZ	YS	E	SS 316 L
Sallica-Leva [85]	Cubic	EC, YS	E	Ti-6Al-4V
Shen [86]	BCC, FCCZ	YS	E	SS 316 L
Smith [87]	BCC, FCCZ	EC, YS, PS	E, F	SS 316 L
Suard [88]	Octet-Truss	EC	E, F	Ti-6Al-4V
Tancogne-Dejean [89]	Octet-Truss	EC, PR	F	SS 316 L
Tsopanos [90]	BCC	EC, YS	E	SS 316 L
Ushijima [91]	BCC	EC, PR	A, F	SS 316 L
Ushijima [45]	BCC	EC, PR, YS	A	SS 316 L
Van Grunsven [92]	Diamond	EC, YS	E	Ti-6Al-4V
Wauthle [93]	Diamond	EC, YS	E	Ti-6Al-4V
Xiao [94]	Rhombic Dodecahedron	EC, YS, PS	E	Ti-6Al-4V
Yan [95]	TPMS Gyroid	YS	E	AlSi10Mg
Yan [96]	TPMS Diamond	EC, YS	E	AlSi10Mg
Yan [97]	TPMS Gyroid	EC, YS	E	SS 316 L
Yan [98]	TPMS Gyroid	EC, YS	E	SS 316 L
Yan [99]	TPMS Gyroid, TPMS Diamond	EC, YS	E	Ti-6Al-4V
Yanez [100]	TPMS Gyroid	EC, YS	E, F	Ti-6Al-4V
Yang [101]	TPMS Gyroid	EC	E, F	Ti-6Al-4V
Zadpoor [102]	Cubic, Diamond, Truncated Cube, Truncated Cuboctahedron, Rhombic Dodecahedron, Rhombicuboctahedron, Truncated Octahedron, Octahedron, BCC, FCC	EC, PR, YS, BS	A	n/a
Zaharin [103]	Cubic, TPMS Gyroid	EC, YS	E, F	Ti-6Al-4V
Zhao [104]	Cubic, Rhombic Dodecahedron, G7	EC, PS	E	Ti-6Al-4V
Zhao [105]	BCC	EC, YS	E	Ti-6Al-4V
Zhu [106]	Truncated Octahedron	PR	A	n/a

across the literature. With all the variations in data due to testing methods, AM process parameters, and materials, the purpose of the assumptions is to isolate the effect of unit cell topology in mechanical property trends.

2.4. LUCIE

The Lattice Unit-cell Characterization Interface for Engineering (LUCIE) was developed in MATLAB as a design tool to compare and visualize mechanical properties of lattice structures based on various unit cell topologies. LUCIE presents a large plot area along with several adjustable settings in order to compare the lattice structure data that was collected from the literature. The data can be sorted by adjusting the range of volume fractions and unit cell sizes that are plotted. Few data points were available for a single volume fraction; so, a range allows for more data to be viewed. Drop-down menus labeled “X Property” and “Y Property” specify which lattice structure properties of interest are to be plotted on the X and Y axis, respectively. Check boxes can then be used to select the type of data (Analytical, FEA, and/or Experimental) and the unit cell topologies that are plotted. Multiple data types and unit cell topologies can be selected to aid in comparison.

The FEA and experimental data collected from the literature search were stored in spreadsheets. Numerical data catalogued the data's source, unit cell topology, mechanical property, volume fraction, unit cell size, numerical property value, units, bulk mechanical property value, and the normalized property value. Regression data catalogued the data source, unit cell topology, mechanical property, volume fraction min/max, unit cell size min/max, and constants (a , b , c) for the power regression equation, see Eq. 2.

Equations for the analytical data were stored explicitly in a MATLAB function. It was typical for these equations to have either the volume fraction or aspect ratio (ratio of strut radius to strut length) as the independent variable. In many cases, algebraic manipulations of the analytical equations were required in order to use volume fraction or aspect ratio as the independent variable.

An example of inputs and outputs for LUCIE is shown in Fig. 3. To use LUCIE, a user must first set the desired data range values and unit cell topologies to be displayed along with data types. Volume fraction and unit cell size are set either with the sliders or the text edit boxes. For both volume fraction, a minimum and maximum value need to be specified so that data can be selected from a range. For unit cell size, either “All” data can be plotted or a range may be selected. For sources that did not directly specify the unit cell size of the test data, the data points are included when “All” unit cell size data is selected. However, if a unit cell size range is specified, only data with a known unit cell size is plotted. The desired properties for the X and Y axes need to be specified along with the types of data and unit cell topologies are to be plotted. Once all settings have been chosen, the MATLAB code filters all of the data so that only data that satisfies the user's specifications are plotted.

In the case where one of the properties selected was volume fraction, the data could be plotted directly, because all the data types were reported, or calculated, as a function of volume fraction. In the case where volume fraction was not selected as one of the properties to be plotted, the properties were calculated by the specified range of volume fraction and unit cell size and then parametrically represented.

In the case of the analytical data type, data was represented by continuous functions. For each specified lattice structure, the two functions that pertain to the selected properties of interest were plotted parametrically with volume fraction as the input parameter.

In the case of the experimental and FEA data types, the data was represented by discrete points, which were first combined into bins by volume fraction. Each bin contained a range of 5% volume fraction, combining any data pertaining to that range. After the data from each property type was sorted into bins, the data could be represented parametrically for each property by volume fraction. In these cases, the

data was plotted using two error bars that show the maximums and minimums of the data in that bin. The location where two error bars intersect denoted the average value. In the case of only a single data point within the bin range error bars were not shown.

3. Results and case studies

3.1. Results of literature compilation

A summary of the type of data and properties for each unit cell topology is shown in Table 3, and the unit cell topologies are illustrated in Table 4. Compiling all the data from 69 papers, 1439 experimental data points were collected across 18 different unit cell topologies. For the experimental data points, 41 % were collected from tabulated values, and the remaining 59 % were extracted from digital images in the original sources using WebPlotDigitizer. In addition, 209 data points for finite element simulations were also collected. The majority of data was available for the effective modulus (compressive) and yield stress of lattice structures; however, there was also some data available in literature for Poisson's ratio, buckling stress, or plateau stress.

As shown in Table 3, the mechanical properties for compiled data include elastic modulus (compressive) (EC), yield stress (YS), Poisson's ratio (PS), buckling stress (BS), and plateau stress (PS). In Table 3, a dash (-) signifies that no reference was found that provided this information for any of the three data types. One limitation of this work, as mentioned previously, is the challenge with inconsistent terminology and methods for computing and reporting mechanical properties. As such, a brief description of each property as we have defined it follows.

Compressive elastic modulus is defined as the slope of the linear portion of the stress-strain curve during the initial loading or the linear portion of the unloading curve during testing, although Ashby et al. [2] suggests that unloading modulus may be a more accurate representation of the structure's performance. Yield stress is defined as the first peak stress for stretch-dominated lattice structures, and is generally the same as the plateau stress for bend-dominated lattice structures [14,28,76]. In a few cases, sources may have instead reported yield stress based on a strain offset as opposed to a first peak or plateau stress. Plateau stress is defined as the average stress value during the cyclical collapse of the bending-dominated lattice structures or during the relatively level stress that occurs in stretch-dominated structures [14,76]. Buckling stress is defined only in the analytical data type because, in general, changes in slope on the stress-strain curve due to yielding or

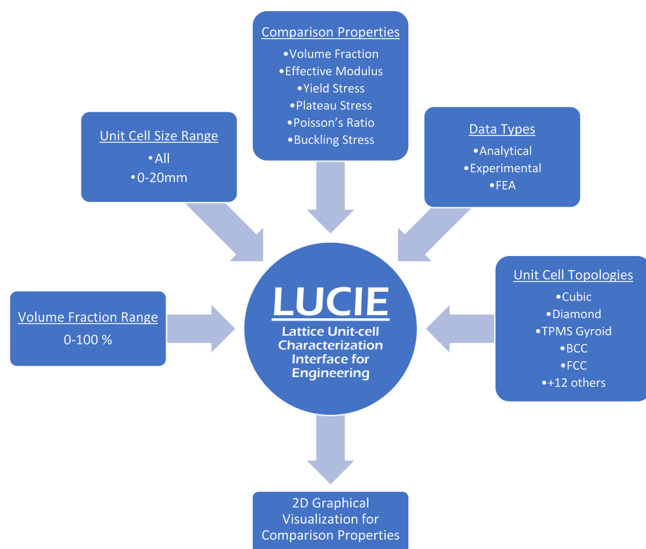


Fig. 3. Schematic showing the inputs and outputs for LUCIE.

Table 3

For each unit cell topology included in LUCIE, there are 6 different properties that can be compared. The data type available for each unit cell topology are denoted by analytical (A), experimental (E), or FEA (F). A dash (-) signifies that no reference was found that provided this information for any of the three data types.

Unit Cell Topology	Volume Fraction	EC	YS	PR	BS	PS
Cubic	A	A, E, F	A, E, F	A, F	A	E
Diamond	A	A, E, F	A, E, F	A, F	A	A, E
Truncated Cube	A	A, E, F	A, E, F	A, F	A	E
Truncated Cuboctahedron	A	A, E, F	E, F	A, F	A	E
Rhombic Dodecahedron	A	A, E, F	E, F	A, F	-	E
Rhombicuboctahedron	A	A, E, F	A, E, F	A, F	-	E
Truncated Octahedron	A	A, F	F	A, F	-	-
Octahedron	A	A, E, F	E, F	A, F	-	-
Octet-Truss	A	A, E, F	A, E	F	-	-
BCC	A	A, E, F	A, E, F	A, E, F	-	E, F
BCCZ	A	A, E, F	E, F	E	-	E, F
FCC	A	A, E	E	A	-	-
FCCZ	A	E	E	-	-	E
F2BCC	A	E	E	-	-	-
F2BCCZ	A	E	E	-	-	-
TPMS Gyroid	-	E, F	E, F	-	-	E
TPMS Diamond	-	E, F	E	-	-	-
G7	-	E	-	-	-	E

Table 4

Name and associated picture for each lattice structure included in LUCIE.

Unit Cell Topology	Image	Unit Cell Topology	Image
Cubic		BCC	
Diamond		BCCZ	
Truncated Cube		FCC	
Truncated Cuboctahedron		FCCZ	
Rhombic Dodecahedron		F2BCC	
Rhombicuboctahedron		F2BCCZ	
Truncated Octahedron		TPMS Gyroid	
Octahedron		TPMS Diamond	
Octet-Truss		G7	

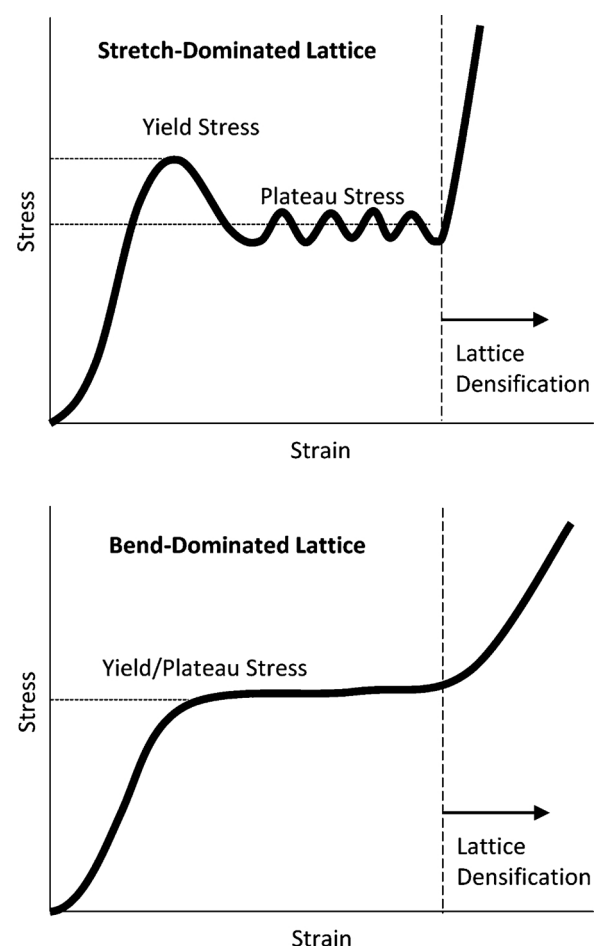


Fig. 4. Typical stress-strain curves for stretch-dominated or bend-dominated structures, labeled with the relevant mechanical property terminology for the data compiled in this work.

buckling are difficult to distinguish. As such, the buckling stress of lattice structures is not reported experimentally. The distinction or classification of stretch- or bend-dominated unit cells is not categorized or recorded within LUCIE, but it is useful to understand what the yield or plateau stress represents in different unit cell topologies.

Fig. 4 illustrates each property and the differences between loading curves for stretch-dominated and bending-dominated truss-like lattice structures. Bend-dominated structures tend to have a peak stress at yield, and then the stress decreases as layers begin to collapse. Stretch-dominated structures tend to maintain more of a plateau in their stress strain curve as the struts yield in tension and collapse prior to densification. Stretch-dominated and bend-dominated lattice structures are determined based on their Maxwell number, which suggests how deformation will occur in the structure [3,113].

Regarding experimental data collected, the data may be grouped in four categories: (1) “non-averaged”, (2) “non-averaged + uncertainty”, (3) “averaged”, and (4) “averaged + uncertainty”.

- “Non-averaged” data points are defined as data points that did not represent an average from experimental replicates and did not include uncertainty reported in the source. These data points are from sources that reported all of the data from their experimental replicates as individual points as opposed to only the average of the data, or from sources that did not have any experimental replicates. In the LUCIE database for experimental data, “non-averaged” accounts for 65.8 % of the data points we collected.

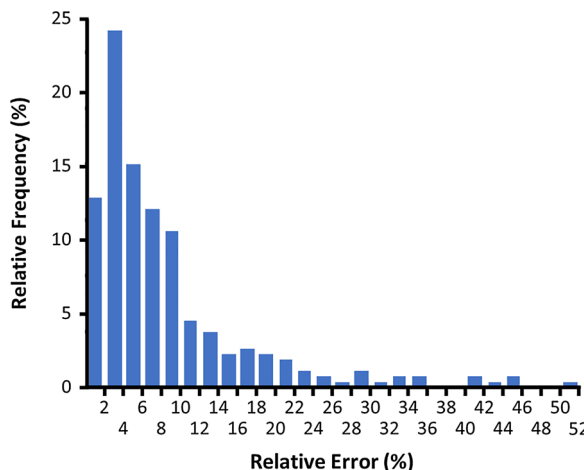


Fig. 5. Relative frequency of uncertainty in experimental data points. Uncertainty is normalized by the nominal value to obtain the relative error. 75 % of the reported uncertainty values had a relative error of less than 10 %.

- “Non-averaged + uncertainty” data points are defined as data points that did not represent an average from experimental replicates but did include uncertainty reported in the source. In a single source, replicates were not reported, but the source estimated the uncertainty based on the testing equipment. In the LUCIE database for experimental data, “non-averaged + uncertainty” accounts for only 0.7 % of the data points we collected.
- “Averaged” data points are defined as data points that represent an average of the experimental replicates but for which an uncertainty value was unavailable. The unavailability of the uncertainty associated with the averaged data points was for one of two reasons: (i) the uncertainty was not reported or (ii) it was not visible for digital image extraction. For example, if uncertainty was reported as error bars on a plot, then the error bars were occasionally hidden by the data point marker they were attached to or other nearby markers, making it impossible to accurately extract the uncertainty. In the LUCIE database for experimental data, “averaged” accounts for 15.8 % of the data points we collected.
- “Averaged + uncertainty” data points are defined as data points that represent an average of the experimental replicates and included an uncertainty value. These data points were often reported as tabulated values (e.g., 10 ± 1 MPa) or on plots that included error bars. In the LUCIE database for experimental data, “averaged + uncertainty” accounts for 17.7 % of the data points we collected.

From the collection of experimental uncertainty, 264 of 1439 data points were reported with uncertainty (18.4 %). A histogram has been created to show the frequency of the relative error for the data points reported with uncertainty; see Fig. 5. The relative error is defined as the uncertainty divided by the nominal value. For example, for a data point 10 ± 1 , the relative error is ± 10 %. In cases where the error bars extracted from digital images were different on the high or low side, the conservative, or larger, error value was taken. From the histogram of the relative error, we find that when the experimental uncertainty was reported, 75 % of the data had an uncertainty of less than 10 %. As there was only a select portion of the data, 18.4 %, for which experimental uncertainty was quantified in the literature, the uncertainty value is not directly accounted for within the LUCIE database. As described in Section 2.4, uncertainty of points shown on a plot within LUCIE denote the maximum and minimum values averaged from the bin of data for that point. As more data becomes available with quantified uncertainty, future revisions allow the user to restrict data to a specific cutoff threshold.

3.2. LUCIE case study 1

Case Study 1 is a demonstration of the output from LUCIE. Fig. 6 shows a comparison of volume fraction and the normalized elastic modulus using analytical, experimental, and FEA data. The unit cell topologies plotted here are the BCC, Diamond, and Truncated Cube for a volume fraction range and unit cell size of 0–50 % and 0–10 mm, respectively, to capture a large range of data. It can be seen that for the analytical Diamond cell data (red), three curves are plotted to reflect analytical results from different sources. In general, these analytical curves represent the experimental and FEA data fairly well at low volume fractions and at higher volume fractions the range of data is much larger. In contrast, other analytical models tend to underpredict or overpredict the experimental and FEA data. For example, in Fig. 6 the analytical BCC curve (blue) underpredicts the experimental data beyond a volume fraction of 0.15. However, the analytical curve for the Truncated Cube overpredicts the experimental data reported for that unit cell topology and diverges from the FEA simulation results.

3.3. LUCIE case study 2

Case Study 2 contains only experimental data from LUCIE; see Fig. 7. This figure plots the volume fraction and yield stress for Diamond, Truncated Cube, Truncated Cuboctahedron, Rhombic Dodecahedron, Rhombicuboctahedron, BCCZ, and TPMS Gyroid unit cell topologies. The ranges of volume fraction and unit cell size were set to 5–40 % and 1–5 mm, respectively. The plot indicates a general area where a particular unit cell topology’s data exists and how it compares to other unit cell topologies and types of data. For example, the Diamond unit cell topology was reported to have a lower yield stress than the Truncated Cube or TPMS Gyroid; however, it was on par with reported data for the Rhombic Dodecahedron. By making these comparisons, a user can easily update the settings in the interface to narrow the search for a particular unit cell topology.

LUCIE can benefit designers by allowing them to easily compare unit cell topologies. For example, based on the plot shown in Fig. 7, a designer who was previously considering a diamond unit cell topology would see that by switching to a TPMS gyroid unit cell topology there are opportunities for further reducing weight or increasing the yield stress value. Specifically, starting from a diamond unit cell topology with a volume fraction of 0.35–0.4, a designer can achieve the same yield stress with nearly 50 % weight savings by switching to a TPMS gyroid unit cell topology with a volume fraction of 0.2. Similarly, by switching from the previously mentioned diamond unit cell to a TPMS gyroid unit cell topology with volume fraction between 0.35–0.4, the normalized yield stress value is increased by 76 % with no change in weight.

3.4. LUCIE case study 3

Case Study 3 illustrates how to use LUCIE as a design tool to aid unit cell selection by providing information to differentiate unit cell topologies and their performance. Consider the design requirements for a lattice structure with a target density, effective normalized modulus, and normalized yield stress of 0.2–0.25, 0.02–0.03, and 0.05 or greater, respectively. LUCIE is used to plot experimental data for volume fraction and elastic modulus of the 18 different available unit cell topologies; see Fig. 8. Next, the user locates the region of interest on the plot according to the design constraints on volume fraction and elastic modulus. The region of interest is highlighted in Fig. 8 by a red box with a dashed line. From this plot we can identify six potential unit cell topologies, whose average effective elastic modulus falls within the region of interest. This reduces our selection from 18 to 6 unit cell topologies: Cubic, BCC, Truncated Cuboctahedron, and Rhombicuboctahedron, TPMS Gyroid, and Octet-Truss.

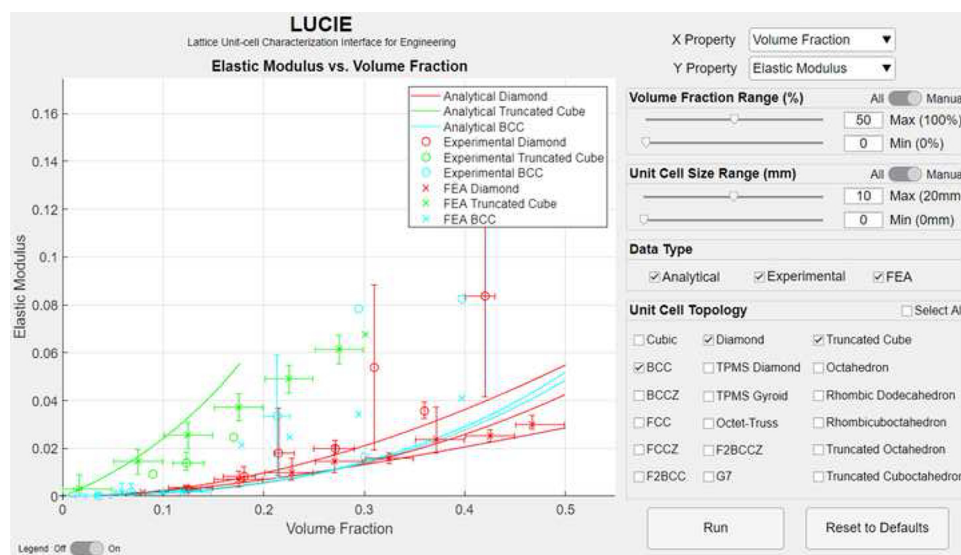


Fig. 6. LUCIE Case Study 1 output comparing analytical, experimental, and FEA data for the BCC, Diamond, and Truncated Cube unit cell topologies. From the output you can visualize differences in analytical models for a single unit cell topology, such as the Diamond, as well as gain a better understanding of relative elastic modulus between unit cell topologies.

A new plot is generated by selecting only the six unit cell topologies identified from Fig. 8, with a comparison of elastic modulus and yield stress with a volume fraction restriction of 0.2–0.25; see Fig. 9. It can be seen that there is a clearer distinction between the possible cells. The Cubic cell has the highest average reported yield stress followed by the TPMS Gyroid, Rhombicuboctahedron, Truncated Cuboctahedron, and finally the BCC. No yield stress data is available in this range for the Octet-Truss. With a stipulation that the normalized yield stress be greater than 0.05, the designer could move forward with either a Cubic, TPMS Gyroid, or Rhombicuboctahedron. One consideration could be the large range of yield stress that has been reported for the TPMS Gyroid, directing a user to further explore how the yield stress can be high or low for similar volume fractions. Further distinction can be considered based on desired print tolerances, unit-cell pore sizes, etc. For example, the Rhombicuboctahedron has more struts, meaning that, for the same volume fraction and unit cell size, the strut diameters and unit cell topology pore sizes will be smaller than those of the Cubic cell. If a small unit cell topology pore size is critical to the application then the Rhombicuboctahedron would likely be a better choice; however, if minimum feature size is a concern, the Cubic unit cell topology has larger strut sizes which could be easier to print and the larger pores enable easier powder removal. For an AM designer, rather than an expensive experimental trial with 18 different unit cell topologies,

LUCIE is able to quickly narrow the search to only three unit cell topologies that could be compared or prepared for further testing, resulting in valuable cost and time savings.

4. Discussion

While the data presented in the interface can be used by designers to compare the lattice structure properties to improve unit cell selection, there were a number of challenges that remain and limitations that exist in the current approach. AM remains a continuously changing and evolving process with a wide range of process parameters, materials, and build strategies still being developed. This work compiled data by unit cell topology, but not by the material or processing conditions. The intended result was not to say that all data for a unit cell topology was processed with a single set of process parameters; rather, it shows the range of mechanical properties that can be achieved with a single unit cell topology. Even the analytical models that have been developed differ based on their underlying assumptions and the experimental data differs even further; see the diamond cell analytical models shown in Fig. 6 as an example.

In cited sources, several reasons for differences between analytical, finite element, and experimental data are suggested. Analytical models tend to overestimate elastic modulus when compared to finite element

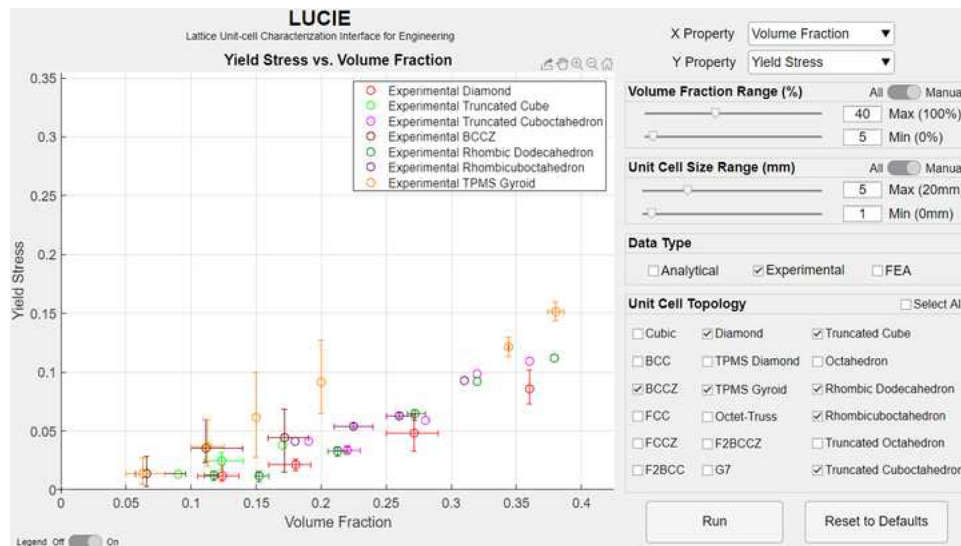


Fig. 7. LUCIE Case Study 2 output shows a comparison of 7 different unit cell topologies and the variability that exists in experimental data. The error bars around a single point represent a small “bin” of data. The point itself represents the average value within the bin, while the error bars denote the maximum and minimum reported values for each property.

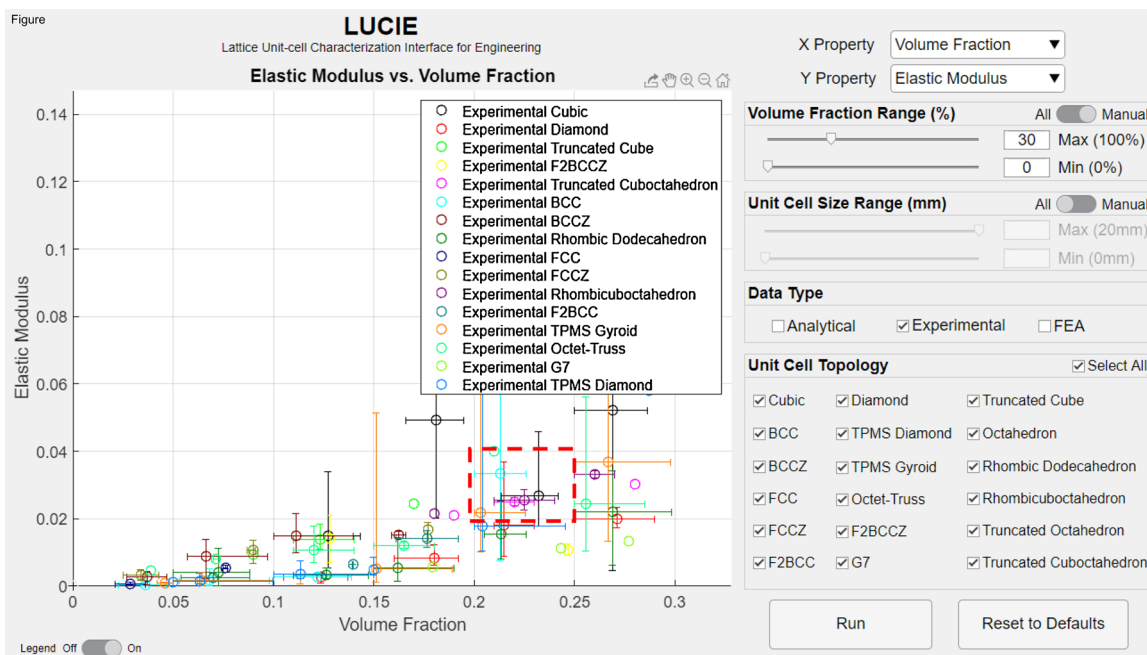


Fig. 8. LUCIE Case Study 3 output from LUCIE for comparison of the lattice structure properties of different unit cell topologies. The red box with a dashed line highlights the region of interest (EC 0.02–0.03 and Volume Fraction 0.2–0.25) for determining appropriate unit cell selection. (For interpretation of the references to colour in this figure legend, the reader is referred to the web version of this article).

and experimental data and deviate more as volume fraction increases. Analytical models derived using the Euler-Bernoulli method ignore shear and rotational inertia which decrease stiffness [41,61,62,64]. Shear and rotational inertia become more influential as volume fraction increases where more unit cell volume exists at strut intersections. Analytical and FEA values for yield stress can overlap if critical struts experience no bending and therefore are unaffected by shear and rotational inertia [61]. Finite element models using the Timoshenko method account for shear and rotational inertia.

As for experimental data compared to analytical and FEA data, it is

stated in the literature that imperfections in the printing process are responsible for the biggest discrepancies. For example, surface roughness as a result of unmelted or semi-melted powder can cause variations in strut radius and cause stress concentrations [52,56–58, 61,62,64,65,103]. Additionally, quality of print for vertical, inclined, and horizontal struts vary, and this is not captured by finite element or analytical models, which assume perfectly cylindrical and homogeneous struts [64]. Meanwhile, strut alignment often differs between experimental and finite element models as well. Analytical and finite element models do not account for slight misalignments among struts

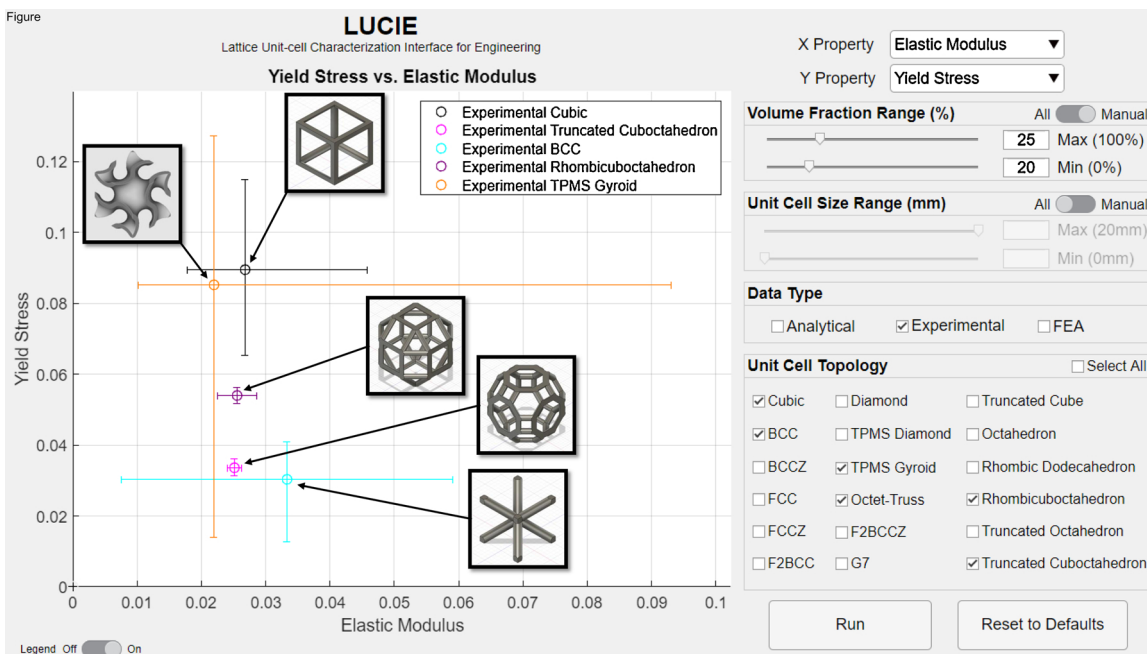


Fig. 9. LUCIE Case Study 3 plot comparison of elastic modulus and yield stress for comparison of the six unit cell topologies that were down selected from Fig. 8. The thumbnails of the unit cell topologies have been added to the plot; from top to bottom they are Cubic, TPMS Gyroid, Rhombicuboctahedron, Truncated Cuboctahedron, BCC, and BCCZ. No yield stress data was available for the Octet-Truss at this volume fraction range.

and loading conditions [52,68]. Other causes for disagreements may be due to the number of unit cells tested (finite or infinite) or lack of accounting for strut interference during densification [62,87].

Different approaches have been proposed to increase the accuracy of analytical and finite element models. Several sources try to account for imperfections in their models by changing the as-designed strut radius to match a geometric average of a physical radius or by applying a randomly varying strut radius [52,88]. One study improved their finite element model by using reconstructed struts based on CT-scans which had greater accuracy over as-designed and average radii models [71]. Having misaligned struts in finite element simulations has also been proposed to improve the model [52].

As another example of the variation that was present in the literature, consider the gyroid data presented in Fig. 7. The range of data that was available from 0.1–0.15 volume fraction had a large range in the reported yield stress as shown by the large vertical error bars. This finding suggests that a difference in testing conditions, build quality, definition of the gyroid, or processing parameters had major effects on the yield stress of the gyroid unit cell topology. The variation seen in the gyroid could lead to several outcomes. First, one researcher could see the data and take it as an argument for standardization of process parameters and testing procedures. While standardization is critical, by combining all the results into a single interface, the range of capabilities of the gyroid are represented. A second researcher could take the result and wish to understand how the gyroid can be tailored to meet a specific yield stress criterion. By reviewing the original literature sources compiled in LUCIE, the ability for researchers to explore the capabilities of the gyroid lattice structure is simplified.

Another factor in the variability of data could be attributed to the variations in testing conditions such as the number of unit cells included in the array, boundary conditions in the compression test, strain rate, etc. For example, ISO 13314:2011, the standard that addresses mechanical testing of porous and cellular metal structures, recommends a periodicity of 10x in each direction in order to minimize the effects from boundary conditions. However, as mechanical testing of lattice structures has not been formalized, many authors do not strictly follow this guideline and test samples with fewer than ten unit cells in any of the three directions. In this work, test samples with fewer than ten unit cells in each direction were not excluded, resulting in data that may be skewed by differences in the impact of boundary conditions on testing results. As with standard materials and testing, consistent standards applicable to lattice structures are needed to ensure that the scientific community—and eventually designers and engineers—can regularize the testing methods to achieve more consistent results.

Another inherent challenge with AM is the design freedom that is available. Because there is so much design freedom, there are infinite minor variations on a single unit cell topology, such as rounding or fillets at node locations, making it impossible to name and track each individual unit cell topology. The purpose of this work is not to say that the optimal unit cell topology is found within the 18 topologies included in LUCIE. In our opinion, there is a large gap between what can be designed and quantified for analysis and what can be printed in metal using current laser and electron beam powder bed fusion technology. AM processes can print complexity that designers would have never dreamed of or imagined previously. However, for the designer to feasibly characterize such infinite possibilities and complexity into a functional and reliable component is currently not possible. The intention of LUCIE is to help bridge this gap by providing a database to allow researchers and designers a better understanding of regular unit cells that have been characterized through analytical, experimental, and finite element analysis. In this work, we have grouped similar unit cell topologies where possible, though minor variations in geometric models do exist. As such, the purpose of LUCIE is visualization of performance trends based on the unit cell type.

Related to the challenge imposed by unit cell topology design freedom, comes the challenge of naming convention. Several authors

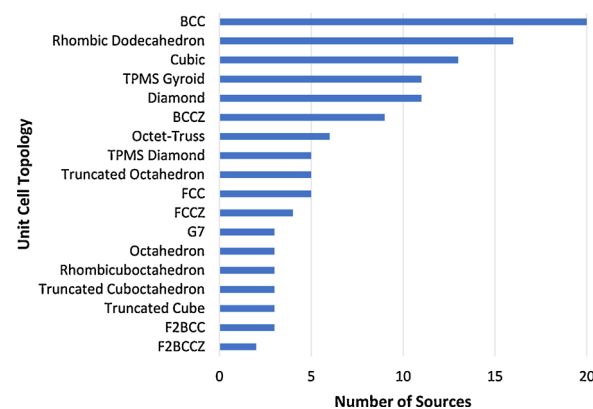


Fig. 10. Number of sources found for each unit cell topology. The results show the amount of lattice structure data available is limited for even more common unit cell topologies.

have tried to address this issue for lattice structures and unit cell topologies and it remains an ongoing battle [22–24]. When compiling our data, the unit cell topology naming conventions were similar; however, variations were seen across different research articles and software libraries. In this work, we have attempted to use the most common name found in literature for describing the unit cell topology.

The amount of data available is increasing all the time but remains limited, especially for some unit cell topologies. In the unit cell selection example, Case Study 3, represented by Figs. 8 and 9, there was lattice structure data available that fit the design requirements; however, in some cases data may not be available because there are many gaps in the published literature. For example, the Octet-Truss was initially identified as a potential candidate in Case Study 3, but no data was available for yield stress in the specified volume fraction range. The focus of this initial work was common unit cell topologies, or those for which more than a single source could be found. As a result, less common and modified versions of common lattice structures were excluded for lack of sufficient data. Fig. 10 shows the number of sources used for each unit cell topology. With the amount of published data increasing all the time, we expect to be able to continue expanding the database for LUCIE and the research community's understanding of the range of mechanical properties that may be achieved with AM lattice structures.

As the focus of this work is identifying the material independent mechanical property trends of lattices structures based on the unit cell topology, all materials were combined through normalization. At present, sorting by material is not available to a front-end user due to the limited amount of data available for each material. With continued expansion of the database for LUCIE, future work may include sorting or categorizing data by material as an option to further refine the results in LUCIE.

Another limitation of LUCIE is that the exact testing conditions (testing machine type, crosshead rate, boundary conditions, etc.) and AM processing parameters are not stored within the current LUCIE database or available to the user on the front-end. For the testing conditions, the information is available in the cited sources. In contrast, in terms of fabrication, few papers report the specific details of the AM process parameters, often due to the proprietary information of the AM machine manufacturer. Of those papers that do report AM process parameters, the amount and type of information that is reported is inconsistent across different sources. The ability to incorporate testing conditions and AM process parameters for each data point in LUCIE in a useful manner was thus limited because each data point represents numerous papers, each with their own testing methods and AM process parameters. Future work for LUCIE could also address how to make the sources for each combined data point more accessible, along with information regarding testing methods and AM process parameters for

comparison of how these factors affect the mechanical properties.

Based on the research articles which have been compiled into the LUCIE database, a number of future directions have been identified for short-term and long-term lattice structure research. In the short-term, testing methods, naming conventions, and standard practices should be developed and standardized in order to allow researchers to collaborate more easily and compare experimental data and analytical and simulation results. The issue of lack of standardization makes it very difficult for researchers to understand the current state when published works are obfuscated by unique naming conventions. Standardization across naming conventions and testing appears to be the low hanging fruit that can help accelerate lattice structure research for AM. In the long-term, as the interest in lattice structures grows, research initiatives should include exploration of:

- 1) Additional experimental loading conditions such as tensile, shear, and fatigue,
- 2) Novel modeling approaches to account for hierarchical complexity,
- 3) Incorporation of manufacturing variability in modeling and simulation,
- 4) Novel unit cell topologies through optimization,
- 5) Post-processing opportunities and effects, and
- 6) Industrial-proven case studies of lattice structure advantages.

Additional methods to model and predict the effect of lattice structures within the full component will be an enabling factor for driving forward industrial applications. As discussed previously, the majority of the present literature is focused on compressive behavior, although most components undergo a variety of loading conditions. Non-compressive behavior, especially cyclic and fatigue loading, is a major concern among researchers for the applications of lattice structures. Finally, learning how to further improve lattice structures with novel topologies or post-processing methods will continue to advance the opportunities available for lattice-enabled components.

There are ongoing efforts to make LUCIE publicly available for all researchers and engineers. Currently, LUCIE can be downloaded as a standalone application for installation on a Windows operating system (see <https://sites.psu.edu/edog/lucie/>). This standalone version requires the MATLAB Compiler Runtime which will be downloaded and installed for free during the installation process, meaning that a MATLAB license is not required to use the application. In addition, ongoing efforts include development of a web-based version of LUCIE that will allow researchers to utilize the application without having to download and maintain an up-to-date version of the application. The intent of the web-based tool is to simplify access to LUCIE with additional plans to allow researchers to be able to submit their own data for incorporation into the database.

5. Closing remarks

Through review of over 69 papers, a comprehensive mechanical property database was compiled and the Lattice Unit-cell Characterization Interface for Engineering (LUCIE) was developed in order to provide Ashby-style plots for unit cell selection of AM lattice structures. Researchers and AM designers stand to benefit from simplified methods to observe and understand unit cell topology effects on lattice structure mechanical properties through LUCIE and similar interfaces and databases. Though the amount of data and lack of testing standards are limiting, ongoing efforts will continue to update the available database and interface with the latest AM research data.

CRediT authorship contribution statement

Bradley Hanks: Visualization, Conceptualization, Methodology, Investigation, Writing - original draft, Writing - review & editing.
Joseph Berthel: Methodology, Software, Formal analysis,

Investigation, Writing - original draft, Writing - review & editing. **Mary Frecker:** Supervision, Writing - review & editing. **Timothy W. Simpson:** Supervision, Writing - review & editing.

Declaration of Competing Interest

The authors declare that they have no known competing financial interests or personal relationships that could have appeared to influence the work reported in this paper.

Acknowledgment

The authors gratefully acknowledge the efforts of the authors of the 69 source papers in modeling, testing, and analyzing lattice structures for additive manufacturing.

Funding

Funding for this research was provided by Penn State's Center for Innovative Materials Processing through Direct Digital Deposition (CIMP-3D).

Appendix A. Supplementary data

Supplementary material related to this article can be found, in the online version, at doi:<https://doi.org/10.1016/j.addma.2020.101301>.

References

- [1] Y. Tang, Y.F. Zhao, A survey of the design methods for additive manufacturing to improve functional performance, *Rapid Prototyp. J.* 22 (2016) 569–590, <https://doi.org/10.1108/RPJ-01-2015-0011>.
- [2] M.F. Ashby, A.G. Evans, N.A. Fleck, L.J. Gibson, J.W. Hutchinson, H. Wadley, *Metal Foams: A Design Guide*, Butterworth-Heinemann, Boston, MA, 2000.
- [3] M. Ashby, The properties of foams and lattices, *Philos. Trans. R. Soc. A Math. Phys. Eng. Sci.* 364 (2006) 15–30, <https://doi.org/10.1098/rsta.2005.1678>.
- [4] L.J. Gibson, M.F. Ashby, *Cellular Solids*, 2nd ed., Cambridge University Press, Cambridge, New York, 1997.
- [5] L.J. Gibson, M.F. Ashby, The mechanics of three-dimensional cellular materials, *Proc. R. Soc. London* 382 (1982) 305–331.
- [6] G. Savio, R. Meneghelli, G. Concheri, Geometric modeling of lattice structures for additive manufacturing, *Rapid Prototyp. J.* 24 (2018) 351–360, <https://doi.org/10.1108/RPJ-07-2016-0122>.
- [7] G. Dong, Y. Tang, Y.F. Zhao, A survey of modeling of lattice structures fabricated by additive manufacturing, *J. Mech. Des.* 139 (2017) 1–13, <https://doi.org/10.1115/1.4037305>.
- [8] S. Watts, D.A. Tortorelli, A geometric projection method for designing three-dimensional open lattices with inverse homogenization, *Int. J. Numer. Methods Eng.* 112 (2017) 1564–1588, <https://doi.org/10.1002/nme.5569>.
- [9] C. Sharpe, C.C. Seepersad, S. Watts, D. Tortorelli, Design of mechanical metamaterials via constrained bayesian optimization, Vol. 2A 44th Des. Autom. Conf., American Society of Mechanical Engineers (2018) 1–11, <https://doi.org/10.1115/DETC2018-85270>.
- [10] B. Hanks, M. Frecker, Lattice structure design for additive manufacturing: unit cell topology optimization, *ASME Int. Des. Eng. Tech. Conf. Comput. Inf. Eng.* (2019) 1–11.
- [11] A. Panesar, M. Abdi, D. Hickman, I. Ashcroft, Strategies for functionally graded lattice structures derived using topology optimisation for Additive Manufacturing, *Addit. Manuf.* 19 (2018) 81–94, <https://doi.org/10.1016/j.addma.2017.11.008>.
- [12] S.M. Ahmadi, S.A. Yavari, R. Wautle, B. Pouran, J. Schrooten, H. Weinans, A.A. Zadpoor, Additively manufactured open-cell porous biomaterials made from six different space-filling unit cells: The mechanical and morphological properties, *Materials (Basel.)* 8 (2015) 1871–1896, <https://doi.org/10.3390/ma8041871>.
- [13] S.Y. Choy, C.-N. Sun, K.F. Leong, J. Wei, Compressive properties of Ti-6Al-4V lattice structures fabricated by selective laser melting: design, orientation and density, *Addit. Manuf.* 16 (2017) 213–224, <https://doi.org/10.1016/j.addma.2017.06.012>.
- [14] M. Leary, M. Mazur, H. Williams, E. Yang, A. Alghamdi, B. Lozanovski, X. Zhang, D. Shidid, L. Farahbod-Sternahl, G. Witt, I. Kelbassa, P. Choong, M. Qian, M. Brandt, Inconel 625 lattice structures manufactured by selective laser melting (SLM): mechanical properties, deformation and failure modes, *Mater. Des.* 157 (2018) 179–199, <https://doi.org/10.1016/j.matdes.2018.06.010>.
- [15] D.S.J. Al-Saeedi, S.H. Masood, M. Faizan-Ur-Rab, A. Alomarrah, P. PonnuSamy, Mechanical properties and energy absorption capability of functionally graded F2BCC lattice fabricated by SLM, *Mater. Des.* 144 (2018) 32–44, <https://doi.org/10.1016/j.matdes.2018.01.059>.

- [16] M.-S. Pham, C. Liu, I. Todd, J. Lertthanasarn, Damage-tolerant architected materials inspired by crystal microstructure, *Nature*. (2019), <https://doi.org/10.1038/s41586-018-0850-3>.
- [17] M. Helou, S. Kara, Design, analysis and manufacturing of lattice structures: an overview, *Int. J. Comput. Integr. Manuf.* 31 (2017) 243–261, <https://doi.org/10.1080/0951192X.2017.1407456>.
- [18] F. Tamburrino, S. Graziosi, M. Bordegoni, The design process of additively manufactured mesoscale lattice structures: a review, *J. Comput. Inf. Sci. Eng.* 18 (2018) 1–16, <https://doi.org/10.1115/1.4040131>.
- [19] X. Wang, S. Xu, S. Zhou, W. Xu, M. Leary, P. Choong, M. Qian, M. Brandt, Y.M. Xie, Topological design and additive manufacturing of porous metals for bone scaffolds and orthopaedic implants: a review, *Biomaterials*. 83 (2016) 127–141, <https://doi.org/10.1016/j.biomaterials.2016.01.012>.
- [20] X.P. Tan, Y.J. Tan, C.S.L. Chow, S.B. Tor, W.Y. Yeong, Metallic powder-bed based 3D printing of cellular scaffolds for orthopaedic implants: a state-of-the-art review on manufacturing, topological design, mechanical properties and biocompatibility, *Mater. Sci. Eng. C*. 76 (2017) 1328–1343, <https://doi.org/10.1016/j.msec.2017.02.094>.
- [21] L. Hao, D. Raymont, C. Yan, A. Hussein, P. Young, Design and additive manufacturing of cellular lattice structures, *5th Int. Conf. Adv. Res. Virtual Rapid Prototyp.* (2011) 249–254, <https://doi.org/10.1201/b11341-40>.
- [22] D. Bhate, C. Penick, L. Ferry, C. Lee, Classification and Selection of Cellular Materials in Mechanical Design: Engineering and Biomimetic Approaches, (2018), pp. 1–27, <https://doi.org/10.3390/designs3010019>.
- [23] M. Fazelpour, J.D. Summers, V.Y. Bluoin, A taxonomy for representing prismatic cellular materials, *ASME 2016, Int. Des. Eng. Tech. Conf. Comput. Inf. Eng. Conf. V02BT03A001*, 2016, <https://doi.org/10.1115/DETC2016-59081>.
- [24] F.W. Zok, R.M. Latture, M.R. Begley, Periodic truss structures, *J. Mech. Phys. Solids* 96 (2016) 184–203, <https://doi.org/10.1016/j.jmps.2016.07.007>.
- [25] A. Schoen, *Infinite Periodic Minimal Surfaces without Self-intersections*, (1970).
- [26] I. Maskery, L. Sturm, A.O. Aremu, A. Panesar, C.B. Williams, C.J. Tuck, R.D. Wildman, I.A. Ashcroft, R.J.M. Hague, Insights into the mechanical properties of several triply periodic minimal surface lattice structures made by polymer additive manufacturing, *Polymer (Guildf.)*. 152 (2018) 62–71, <https://doi.org/10.1016/j.polymer.2017.11.049>.
- [27] D. Bhate, Four questions in cellular material design, *Materials (Basel)*. 12 (2019), <https://doi.org/10.3390/ma12071060>.
- [28] T. Macanachie, M. Leary, B. Lozanovski, X. Zhang, M. Qian, O. Faruque, M. Brandt, SLM lattice structures: properties, performance, applications and challenges, *Mater. Des.* (2019) 108137, , <https://doi.org/10.1016/j.matdes.2019.108137>.
- [29] EOS, Materials for Metal Additive Manufacturing, (2019) (n.d.). <https://www.eos.info/material-m> (Accessed 29 August 2019).
- [30] Renishaw, Data Sheets - Additive Manufacturing, (2019) (n.d.). <https://www.renishaw.com/en/data-sheets-additive-manufacturing-17862> (Accessed 29 August 2019).
- [31] A.O. Aremu, I. Maskery, C. Tuck, I.A. Ashcroft, R.D. Wildman, R.I. Hague, A comparative Finite Element study of cubic unit cells for Selective Laser Melting, *Int. Solid Free. Fabr. Symp.* (2014) 1238–1249.
- [32] H. Brodin, J. Saarimäki, Mechanical properties of lattice truss structures made of a selective laser melted superalloy, *13th Int. Conf. Fract.* (2013) 1–10, <https://doi.org/10.1115/GT2013-95878>.
- [33] R. Gümruk, R.A.W. Mines, S. Karadeniz, Static mechanical behaviours of stainless steel micro-lattice structures under different loading conditions, *Mater. Sci. Eng. A*. 586 (2013) 392–406, <https://doi.org/10.1016/j.msea.2013.07.070>.
- [34] R. Hedayati, M. Sadighi, M. Mohammadi-Aghdam, H. Hosseini-Toudeshky, Comparison of elastic properties of open-cell metallic biomaterials with different unit cell types, *J. Biomed. Mater. Res. - Part B Appl. Biomater.* 106 (2018) 386–398, <https://doi.org/10.1002/jbm.b.33854>.
- [35] D. Kang, S. Park, Y. Son, S.H. Kim, I. Kim, Multi-lattice inner structures for high-strength and light-weight in metal selective laser melting process, *Mater. Des.* 175 (2019) 107786, , <https://doi.org/10.1016/j.matdes.2019.107786>.
- [36] S.J. Li, L.E. Murr, X.Y. Cheng, Z.B. Zhang, Y.L. Hao, R. Yang, F. Medina, R.B. Wicker, Compression fatigue behavior of Ti-6Al-4V mesh arrays fabricated by electron beam melting, *Acta Mater.* 60 (2012) 793–802, <https://doi.org/10.1016/j.actamat.2011.10.051>.
- [37] S.A. Yavari, R. Wauthle, J. Van Der Stok, A.C. Riemsdag, M. Janssen, M. Mulier, J.P. Kruth, J. Schrooten, H. Weinans, A.A. Zadpoor, Fatigue behavior of porous biomaterials manufactured using selective laser melting, *Mater. Sci. Eng. C*. 33 (2013) 4849–4858, <https://doi.org/10.1016/j.msec.2013.08.006>.
- [38] S.A. Yavari, S.M. Ahmadi, R. Wauthle, B. Pouran, J. Schrooten, H. Weinans, A.A. Zadpoor, Relationship between unit cell type and porosity and the fatigue behavior of selective laser melted meta-biomaterials, *J. Mech. Behav. Biomed. Mater.* 43 (2015) 91–100, <https://doi.org/10.1016/j.jmbbm.2014.12.015>.
- [39] S. McKown, Y. Shen, W.K. Brookes, C.J. Sutcliffe, W.J. Cantwell, G.S. Langdon, G.N. Nurick, M.D. Theobald, The quasi-static and blast loading response of lattice structures, *Int. J. Impact Eng.* 35 (2008) 795–810, <https://doi.org/10.1016/j.ijimpeng.2007.10.005>.
- [40] Z. Ozdemir, E. Hernandez-Nava, A. Tyas, J.A. Warren, S.D. Fay, R. Goodall, I. Todd, H. Askes, Energy absorption in lattice structures in dynamics: experiments, *Int. J. Impact Eng.* 89 (2016) 49–61, <https://doi.org/10.1016/j.ijimpeng.2015.10.007>.
- [41] Z. Ozdemir, A. Tyas, R. Goodall, H. Askes, Energy absorption in lattice structures in dynamics: nonlinear FE simulations, *Int. J. Impact Eng.* 102 (2017), <https://doi.org/10.1016/j.ijimpeng.2016.11.016>.
- [42] C.I. Hammetter, R.G. Rinaldi, F.W. Zok, Pyramidal lattice structures for high strength and energy absorption, *J. Appl. Mech.* 80 (2013) 041015, , <https://doi.org/10.1115/1.4007865>.
- [43] J. Niu, H.L. Choo, W. Sun, S.H. Mok, Analytical Solution and experimental study Young's modulus of SLM-fabricated lattice structure with triangular unit cells, *J. Manuf. Sci. Eng.* (2018), <https://doi.org/10.1115/1.4026441>.
- [44] S.I. Park, D.W. Rosen, S. kyum Choi, C.E. Duty, Effective mechanical properties of lattice material fabricated by material extrusion additive manufacturing, *Addit. Manuf.* 1 (2014) 12–23, <https://doi.org/10.1016/j.addma.2014.07.002>.
- [45] K. Ushijima, W.J. Cantwell, R.A.W. Mines, S. Tsopanos, M. Smith, An investigation into the compressive properties of stainless steel micro-lattice structures, *J. Sandw. Struct. Mater.* 13 (2011) 303–329, <https://doi.org/10.1177/1099636210380997>.
- [46] V.S. Deshpande, N.A. Fleck, M.F. Ashby, Effective properties of the octet-truss lattice material, *J. Mech. Phys. Solids* 49 (2001) 1747–1769, [https://doi.org/10.1016/S0022-5096\(01\)00010-2](https://doi.org/10.1016/S0022-5096(01)00010-2).
- [47] S.M. Ahmadi, G. Campoli, S. Amin Yavari, B. Sajadi, R. Wauthle, J. Schrooten, H. Weinans, A.A. Zadpoor, Mechanical behavior of regular open-cell porous biomaterials made of diamond lattice unit cells, *J. Mech. Behav. Biomed. Mater.* 34 (2014) 106–115, <https://doi.org/10.1016/j.jmbbm.2014.02.003>.
- [48] S. Arabnejad, R. Burnett Johnston, J.A. Pura, B. Singh, M. Tanzer, D. Pasini, High-strength porous biomaterials for bone replacement: a strategy to assess the interplay between cell morphology, mechanical properties, bone ingrowth and manufacturing constraints, *Acta Biomater.* 30 (2016) 345–356, <https://doi.org/10.1016/j.actbio.2015.10.048>.
- [49] A. Ataei, Y. Li, M. Brandt, C. Wen, Ultrahigh-strength titanium gyroid scaffolds manufactured by selective laser melting (SLM) for bone implant applications, *Acta Mater.* 158 (2018) 354–368, <https://doi.org/10.1016/j.actamat.2018.08.005>.
- [50] C. Beyer, D. Figueiroa, Design and analysis of lattice structures for additive manufacturing, *J. Manuf. Sci. Eng.* 138 (2016) 121014, , <https://doi.org/10.1115/1.4033957>.
- [51] F.S.L. Bobbert, K. Lietaert, A.A. Eftekhar, B. Pouran, S.M. Ahmadi, H. Weinans, A.A. Zadpoor, Additively manufactured metallic porous biomaterials based on minimal surfaces: a unique combination of topological, mechanical, and mass transport properties, *Acta Biomater.* 53 (2017) 572–584, <https://doi.org/10.1016/j.actbio.2017.02.024>.
- [52] M.S. Borleffs, Finite Element Modeling To Predict Bulk Mechanical Properties of 3D Printed Metal Foams, TU Delft, 2012, <http://resolver.tudelft.nl/uuid:551dee76-2301-4f77-ba6e-230d32e8c58f>.
- [53] S.L. Campanelli, N. Contuzzi, A.D. Ludovico, F. Caiazzo, F. Cardaropoli, V. Sergi, Manufacturing and characterization of Ti6Al4V lattice components manufactured by selective laser melting, *Materials (Basel)*. 7 (2014) 4803–4822, <https://doi.org/10.3390/ma7064803>.
- [54] X.Y. Cheng, S.J. Li, L.E. Murr, Z.B. Zhang, Y.L. Hao, R. Yang, F. Medina, R.B. Wicker, Compression deformation behavior of Ti-6Al-4V alloy with cellular structures fabricated by electron beam melting, *J. Mech. Behav. Biomed. Mater.* 16 (2012) 153–162, <https://doi.org/10.1016/j.jmbbm.2012.10.005>.
- [55] C. de Formanoir, M. Suard, R. Dendievle, G. Martin, S. Godet, Improving the mechanical efficiency of electron beam melted titanium lattice structures by chemical etching, *Addit. Manuf.* 11 (2016) 71–76, <https://doi.org/10.1016/j.addma.2016.05.001>.
- [56] R. Gümruk, R.A.W. Mines, Compressive behaviour of stainless steel micro-lattice structures, *Int. J. Mech. Sci.* 68 (2013) 125–139, <https://doi.org/10.1016/j.ijmecsci.2013.01.006>.
- [57] C. Han, C. Yan, S. Wen, T. Xu, S. Li, J. Liu, Q. Wei, Y. Shi, Effects of the unit cell topology on the compression properties of porous Co-Cr scaffolds fabricated via selective laser melting, *Rapid Prototyp. J.* 23 (2017) 16–27, <https://doi.org/10.1108/RPJ-08-2015-0114>.
- [58] O.L.A. Harrysson, O. Cansizoglu, D.J. Marcellin-Little, D.R. Cormier, H.A. West, Direct metal fabrication of titanium implants with tailored materials and mechanical properties using electron beam melting technology, *Mater. Sci. Eng. C*. 28 (2008) 366–373, <https://doi.org/10.1016/j.msec.2007.04.022>.
- [59] H. Bin Hasib, Mechanical Behavior of Non-stochastic Ti-6Al-4V Cellular Structures Produced via Electron beam Melting (EBM), North Carolina State University, 2011, <https://doi.org/10.1017/CBO9781107415324.004>.
- [60] Z.Z. He, F.C. Wang, Y.B. Zhu, H.A. Wu, H.S. Park, Mechanical properties of copper octet-truss nanolattices, *J. Mech. Phys. Solids* 101 (2017) 133–149, <https://doi.org/10.1016/j.jmps.2017.01.019>.
- [61] R. Hedayati, M. Sadighi, M. Mohammadi-Aghdam, A.A. Zadpoor, Mechanics of additively manufactured porous biomaterials based on the rhombicuboctahedron unit cell, *J. Mech. Behav. Biomed. Mater.* 53 (2016) 272–294, <https://doi.org/10.1016/j.jmbbm.2015.07.013>.
- [62] R. Hedayati, M. Sadighi, M. Mohammadi-Aghdam, A.A. Zadpoor, Mechanical properties of regular porous biomaterials made from truncated cube repeating unit cells: analytical solutions and computational models, *Mater. Sci. Eng. C*. 60 (2016) 163–183, <https://doi.org/10.1016/j.msec.2015.11.001>.
- [63] R. Hedayati, M. Sadighi, M. Mohammadi-Aghdam, A.A. Zadpoor, Effect of mass multiple counting on the elastic properties of open-cell regular porous biomaterials, *Mater. Des.* 89 (2016) 9–20, <https://doi.org/10.1016/j.matdes.2015.09.052>.
- [64] R. Hedayati, M. Sadighi, M. Mohammadi-Aghdam, A.A. Zadpoor, Mechanical behavior of additively manufactured porous biomaterials made from truncated cuboctahedron unit cells, *Int. J. Mech. Sci.* 106 (2016) 19–38, <https://doi.org/10.1016/j.ijmecsci.2015.11.033>.
- [65] R. Hedayati, M. Sadighi, M. Mohammadi-Aghdam, A.A. Zadpoor, Analytical relationships for the mechanical properties of additively manufactured porous biomaterials based on octahedral unit cells, *Appl. Math. Model.* 46 (2017) 408–422, <https://doi.org/10.1016/j.apm.2017.01.076>.
- [66] P. Heinl, L. Müller, C. Körner, R.F. Singer, F.A. Müller, Cellular Ti-6Al-4V

- structures with interconnected macro porosity for bone implants fabricated by selective electron beam melting, *Acta Biomater.* 4 (2008) 1536–1544, <https://doi.org/10.1016/j.actbio.2008.03.013>.
- [67] P. Heinl, C. Körner, R.F. Singer, Selective electron beam melting of cellular titanium: mechanical properties, *Adv. Eng. Mater.* 10 (2008) 882–888, <https://doi.org/10.1002/adem.200800137>.
- [68] M. Helou, S. Vongbunyong, S. Kara, Finite element analysis and validation of cellular structures, *Procedia CIRP.* 50 (2016) 94–99, <https://doi.org/10.1016/j.procir.2016.05.018>.
- [69] A.Y. Hussein, *The Development of Lightweight Cellular Structures for Metal Additive Manufacturing*, University of Exeter, 2013.
- [70] M. Leary, M. Maxur, J. Elambasseri, M. Matthew, T. Chirent, Y. Sun, M. Qian, M. Easton, M. Brandt, Selective laser melting (SLM) of AlSi12Mg lattice structures, *Mater. Des.* 98 (2016) 119–161, <https://doi.org/10.1016/B978-0-08-100433-3.00005-1>.
- [71] H. Lei, C. Li, J. Meng, H. Zhou, Y. Liu, X. Zhang, P. Wang, D. Fang, Evaluation of compressive properties of SLM-fabricated multi-layer lattice structures by experimental test and µ-CT-based finite element analysis, *Mater. Des.* 169 (2019) 107685, <https://doi.org/10.1016/j.matesdes.2019.107685>.
- [72] C. Li, H. Lei, Y. Liu, X. Zhang, J. Xiong, H. Zhou, D. Fang, Crushing behavior of multi-layer metal lattice panel fabricated by selective laser melting, *Int. J. Mech. Sci.* 145 (2018) 389–399, <https://doi.org/10.1016/j.ijmecsci.2018.07.029>.
- [73] S.J. Li, Q.S. Xu, Z. Wang, W.T. Hou, Y.L. Hao, R. Yang, L.E. Murr, Influence of cell shape on mechanical properties of Ti-6Al-4V meshes fabricated by electron beam melting method, *Acta Biomater.* 10 (2014) 4537–4547, <https://doi.org/10.1016/j.actbio.2014.06.010>.
- [74] Y.J. Liu, H.L. Wang, S.J. Li, S.G. Wang, W.J. Wang, W.T. Hou, Y.L. Hao, R. Yang, L.C. Zhang, Compressive and fatigue behavior of beta-type titanium porous structures fabricated by electron beam melting, *Acta Mater.* 126 (2017) 58–66, <https://doi.org/10.1016/j.actamat.2016.12.052>.
- [75] Y.J. Liu, S.J. Li, H.L. Wang, W.T. Hou, Y.L. Hao, R. Yang, T.B. Sercombe, L.C. Zhang, Microstructure, defects and mechanical behavior of beta-type titanium porous structures manufactured by electron beam melting and selective laser melting, *Acta Mater.* 113 (2016) 56–67, <https://doi.org/10.1016/j.actamat.2016.04.029>.
- [76] M. Mazur, M. Leary, S. Sun, M. Vcelka, D. Shidid, M. Brandt, Deformation and failure behaviour of Ti-6Al-4V lattice structures manufactured by selective laser melting (SLM), *Int. J. Adv. Manuf. Technol.* 84 (2016) 1391–1411, <https://doi.org/10.1007/s00170-015-7655-4>.
- [77] R.A.W. Mines, S. Tsopanios, Y. Shen, R. Hasan, S.T. McKown, Drop weight impact behaviour of sandwich panels with metallic micro lattice cores, *Int. J. Impact Eng.* 60 (2013) 120–132, <https://doi.org/10.1016/j.ijimpeng.2013.04.007>.
- [78] L. Mullen, R.C. Stamp, W.K. Brooks, E. Jones, C.J. Sutcliffe, Selective laser melting: a regular unit cell approach for the manufacture of porous, titanium, bone ingrowth constructs, suitable for orthopedic applications, *J. Biomed. Mater. Res. - Part B Appl. Biomater.* 89 (2009) 325–334, <https://doi.org/10.1002/jbm.b.31219>.
- [79] L.E. Murr, K.N. Amato, S.J. Li, Y.X. Tian, X.Y. Cheng, S.M. Gaytan, E. Martinez, P.W. Shindo, F. Medina, R.B. Wicker, Microstructure and mechanical properties of open-cellular biomaterials prototypes for total knee replacement implants fabricated by electron beam melting, *J. Mech. Behav. Biomed. Mater.* 4 (2011) 1396–1411, <https://doi.org/10.1016/j.jmbbm.2011.05.010>.
- [80] L.E. Murr, S.M. Gaytan, F. Medina, H. Lopez, E. Martinez, B.I. Machado, D.H. Hernandez, L. Martinez, M.I. Lopez, R.B. Wicker, J. Bracke, Next-generation biomedical implants using additive manufacturing of complex, cellular and functional mesh arrays, *Philos. Trans. R. Soc. A Math. Phys. Eng. Sci.* 368 (2010) 1999–2032, <https://doi.org/10.1098/rsta.2010.0010>.
- [81] L. Murr, S. Li, Y. Tian, K. Amato, E. Martinez, F. Medina, Open-cellular co-base and ni-base superalloys fabricated by electron beam melting, *Materials (Basel).* 4 (2010) 782–790, <https://doi.org/10.3390/ma4040782>.
- [82] J. Parthasarathy, B. Starly, S. Raman, A. Christensen, Mechanical evaluation of porous titanium (Ti6Al4V) structures with electron beam melting (EBM), *J. Mech. Behav. Biomed. Mater.* 3 (2010) 249–259, <https://doi.org/10.1016/j.jmbbm.2009.10.006>.
- [83] E. Ptochos, G. Labeas, Elastic modulus and Poisson's ratio determination of micro-lattice cellular structures by analytical, numerical and homogenisation methods, *J. Sandw. Struct. Mater.* 14 (2012), <https://doi.org/10.1177/1099636212444285>.
- [84] O. Rehme, C. Emmelmann, Rapid manufacturing of lattice structures with selective laser melting, *Laser-Based Micropackaging.* 6107 (2006) 61070K, <https://doi.org/10.1117/12.645848>.
- [85] E. Salicula-Leva, A.L. Jardini, J.B. Fogagnolo, Microstructure and mechanical behavior of porous Ti-6Al-4V parts obtained by selective laser melting, *J. Mech. Behav. Biomed. Mater.* 26 (2013) 98–108, <https://doi.org/10.1016/j.jmbbm.2013.05.011>.
- [86] Y. Shen, S. McKown, S. Tsopanios, C.J. Sutcliffe, R.A.W. Mines, W.J. Cantwell, The mechanical properties of sandwich structures based on metal lattice architectures, *J. Sandw. Struct. Mater.* 12 (2010) 159–180, <https://doi.org/10.1177/1099636209104536>.
- [87] M. Smith, Z. Guan, W.J. Cantwell, Finite element modelling of the compressive response of lattice structures manufactured using the selective laser melting technique, *Int. J. Mech. Sci.* 67 (2013) 28–41, <https://doi.org/10.1016/j.ijmecsci.2012.12.004>.
- [88] M. Suard, Characterization and Optimization of Lattice Structures Made by Electron beam Melting, Université De Grenoble, 2015, https://www.researchgate.net/publication/286677530_Characterization_and_optimization_of_lattice_structures_made_by_Electron_Beam_Melting.
- [89] T. Tancogne-Dejean, A.B. Spierings, D. Mohr, Additively-manufactured metallic micro-lattice materials for high specific energy absorption under static and dynamic loading, *Acta Mater.* 116 (2016) 14–28, <https://doi.org/10.1016/j.actamat.2016.05.054>.
- [90] S. Tsopanios, R.A.W. Mines, S. McKown, Y. Shen, W.J. Cantwell, W. Brooks, C.J. Sutcliffe, The influence of processing parameters on the mechanical properties of selectively laser melted stainless steel microlattice structures, *J. Manuf. Sci. Eng.* 132 (2010) 1–12, <https://doi.org/10.1115/1.4001743>.
- [91] K. Ushijima, W.J. Cantwell, D.H. Chen, Prediction of the mechanical properties of micro-lattice structures subjected to multi-axial loading, *Int. J. Mech. Sci.* 68 (2013) 47–55, <https://doi.org/10.1016/j.ijmecsci.2012.12.017>.
- [92] W. van Grunsven, E. Hernandez-Nava, G. Reilly, R. Goodall, Fabrication and mechanical characterisation of titanium lattices with graded porosity, *Metals (Basel).* 4 (2014) 401–409, <https://doi.org/10.3390/met4030401>.
- [93] R. Wauthle, B. Vrancken, B. Beynaerts, K. Jorissen, J. Schrooten, J.-P. Kruth, J. Van Humbeeck, Effects of build orientation and heat treatment on the microstructure and mechanical properties of selective laser melted Ti6Al4V lattice structures, *Addit. Manuf.* 5 (2015) 77–84, <https://doi.org/10.1016/j.addma.2014.12.008>.
- [94] L. Xiao, W. Song, C. Wang, H. Liu, H. Tang, J. Wang, Mechanical behavior of open-cell rhombic dodecahedron Ti-6Al-4V lattice structure, *Mater. Sci. Eng. A.* 640 (2015) 375–384, <https://doi.org/10.1016/j.msea.2015.06.018>.
- [95] C. Yan, L. Hao, A. Hussein, P. Young, J. Huang, W. Zhu, Microstructure and mechanical properties of aluminum alloy cellular lattice structures manufactured by direct metal laser sintering, *Mater. Sci. Eng. A.* 628 (2015) 238–246, <https://doi.org/10.1016/j.msea.2015.01.063>.
- [96] C. Yan, L. Hao, A. Hussein, S.L. Bubb, P. Young, D. Raymont, Evaluation of lightweight AlSi10Mg periodic cellular lattice structures fabricated via direct metal laser sintering, *J. Mater. Process. Technol.* 214 (2014) 856–864, <https://doi.org/10.1016/j.jmatprotec.2013.12.004>.
- [97] C. Yan, L. Hao, A. Hussein, D. Raymont, Evaluations of cellular lattice structures manufactured using selective laser melting, *Int. J. Mach. Tools Manuf.* 62 (2012) 32–38, <https://doi.org/10.1016/j.ijmachtools.2012.06.002>.
- [98] C. Yan, L. Hao, A. Hussein, P. Young, D. Raymont, Advanced lightweight 316L stainless steel cellular lattice structures fabricated via selective laser melting, *Mater. Des.* 55 (2014) 533–541, <https://doi.org/10.1016/j.matesdes.2013.10.027>.
- [99] C. Yan, L. Hao, A. Hussein, P. Young, Ti-6Al-4V triply periodic minimal surface structures for bone implants fabricated via selective laser melting, *J. Mech. Behav. Biomed. Mater.* 51 (2015) 61–73, <https://doi.org/10.1016/j.jmbbm.2015.06.024>.
- [100] A. Yáñez, A. Cuadrado, O. Martel, H. Afonso, D. Monopoli, Gyroid porous titanium structures: a versatile solution to be used as scaffolds in bone defect reconstruction, *Mater. Des.* 140 (2018) 21–29, <https://doi.org/10.1016/j.matesdes.2017.11.050>.
- [101] E. Yang, M. Leary, B. Lozanovski, D. Downing, M. Mazur, A. Sarker, A. Khorasani, A. Jones, T. Maconachie, S. Bateman, M. Easton, M. Qian, P. Choong, M. Brandt, Effect of geometry on the mechanical properties of Ti-6Al-4V Gyroid structures fabricated via SLM: a numerical study, *Mater. Des.* 184 (2019) 108165, , <https://doi.org/10.1016/j.matesdes.2019.108165>.
- [102] A.A. Zadpoor, R. Hedayati, Analytical relationships for prediction of the mechanical properties of additively manufactured porous biomaterials, *J. Biomed. Mater. Res. - Part A.* 104 (2016) 3164–3174, <https://doi.org/10.1002/jbm.a.35855>.
- [103] H.A. Zaharin, A.M.A. Rani, F.I. Azam, T.L. Ginta, N. Sallih, A. Ahmad, N.A. Yunus, T.Z.A. Zulkifli, Effect of unit cell type and pore size on porosity and mechanical behavior of additively manufactured Ti6Al4V scaffolds, *Materials (Basel).* 11 (2018), <https://doi.org/10.3390/ma11122402>.
- [104] S. Zhao, S.J. Li, W.T. Hou, Y.L. Hao, R. Yang, R.D.K. Misra, The influence of cell morphology on the compressive fatigue behavior of Ti-6Al-4V meshes fabricated by electron beam melting, *J. Mech. Behav. Biomed. Mater.* 59 (2016) 251–264, <https://doi.org/10.1016/j.jmbbm.2016.01.034>.
- [105] M. Zhao, F. Liu, G. Fu, D.Z. Zhang, T. Zhang, H. Zhou, Improved mechanical properties and energy absorption of BCC lattice structures with triply periodic minimal surfaces fabricated by SLM, *Materials (Basel).* 11 (2018), <https://doi.org/10.3390/ma11122411>.
- [106] H.X. Zhu, J.F. Knott, N.J. Mills, Analysis of the elastic properties of open-cell foams with tetrakaidecahedral cells, *J. Mech. Phys. Solids* 45 (1997) 319–343, [https://doi.org/10.1016/S0022-5096\(96\)00090-7](https://doi.org/10.1016/S0022-5096(96)00090-7).
- [107] A. Rohatgi, WebPlotDigitizer, (2019) <https://automeris.io/WebPlotDigitizer>.
- [108] D. Devron, S.R. Fursa, A.L. Malcolm, Intercoder reliability and validity of WebPlotDigitizer in extracting graphed data, *Behav. Modif.* 41 (2017) 323–339, <https://doi.org/10.1177/0145445516673998>.
- [109] M. Moeyaert, D. Maggin, J. Verkuilen, Reliability, validity, and usability of data extraction programs for single-case research designs, *Behav. Modif.* 40 (2016) 874–900, <https://doi.org/10.1177/0145445516645763>.
- [110] B.U. Burda, E.A. O'Connor, E.M. Webber, N. Redmond, L.A. Perdue, Estimating data from figures with a Web-based program: considerations for a systematic review, *Res. Synth. Methods* 8 (2017) 258–262, <https://doi.org/10.1002/jrsm.1232>.
- [111] G.B. McBride, A Proposal for Strength-of-agreement Criteria for Lins Concordance Correlation Coefficient, NIWA Client Rep. HAM2005-06, (2005).
- [112] Desmos Online Calculator, (2019) (Accessed 10 January 2019), <https://www.desmos.com/calculator/7yuoxjowmx>.
- [113] J.C. Maxwell, XLV, On reciprocal figures and diagrams of forces, London, Edinburgh, Dublin Philos. Mag. J. Sci. 27 (1864) 250–261, <https://doi.org/10.1080/1478644640864363>.